Article

Exploiting Anyonic Behavior of Quasicrystals for Topological Quantum Computing

Marcelo Amaral *, **David Chester**, **Fang Fang** and **Klee Irwin**

Quantum Gravity Research, Los Angeles, CA 90290, USA
***** Correspondence: marcelo@quantumgravityresearch.org

Abstract: The concrete realization of topological quantum computing using low-dimensional quasi-particles, known as anyons, remains one of the important challenges of quantum computing. A topological quantum computing platform promises to deliver more robust qubits with additional hardware-level protection against errors that could lead to the desired large-scale quantum computation. We propose quasicrystal materials as such a natural platform and show that they exhibit anyonic behavior that can be used for topological quantum computing. Different from anyons, quasicrystals are already implemented in laboratories. In particular, we study the correspondence between the fusion Hilbert spaces of the simplest non-abelian anyon, the Fibonacci anyons, and the tiling spaces of the one-dimensional Fibonacci chain and the two-dimensional Penrose tiling quasicrystals. A concrete encoding on these tiling spaces of topological quantum information processing is also presented by making use of inflation and deflation of such tiling spaces. While we outline the theoretical basis for such a platform, details on the physical implementation remain open.

Keywords: topological quantum computing; anyons; quasicrystals; quasicrystalline codes; tiling spaces

1. Introduction

While quantum computers have been experimentally realized, obtaining large-scale fault-tolerant quantum computation still remains a challenge. Since qubits are very sensitive to the environment, it is necessary to solve the problem of decoherence [1]. Software algorithms have been proposed by researchers in the field [2–6]. A comparative study with the pros and cons of various quantum computing models is reviewed in [7]. The reviews mentioned highlight the difficulty with scalable quantum error corrections and point out the need for different approaches. A different seminal solution is to add hardware-level error correction via topological quantum computation (TQC) [8,9]. In particular, non-abelian anyons can provide universal quantum computation [8]. Theoretically, low-dimensional anyonic systems are a hallmark topological phase of matter, which could be used for TQC if a concrete implementation could be achieved. While abelian anyons have been experimentally realized [10], concrete evidence of non-abelian anyons still remains elusive. Interestingly, if topological quantum computer hardware can be implemented, additional software-level error correction can be added [11].

The Chern–Simons theory, when applied to the fractional quantum Hall effect and lattice models such as the toric code, constitutes theoretical frameworks for using anyons for TQC [8,9]. These systems support emergent quasiparticle excitations that show anyonic or fractional statistics. The fusion rules and braid properties of anyons are useful for implementing TQC. The quasiparticles that encode the topological information define the structure of the fusion Hilbert space. In the Chern–Simons theory, anyons are classified by an integer parameter called the level k, which appears in the action of the theory. There are infinite levels; $k = 2$ defines Abelian anyons, while greater levels define non-Abelian anyons. The Fibonacci anyon is the quintessential and simplest non-abelian anyon at

the level $k = 3$ [8,9]. For our purposes, the fusion Hilbert space for Fibonacci anyons is described by the Fibonacci C^*-algebra [12].

Due to the potential of TQC and the experimental difficulty of implementing non-Abelian anyons, it is worth understanding what forms of TQC are possible in general. Previously, we co-authored a non-anyonic proposal of TQC from three-dimensional topology [13] and discussed their associated character varieties [14]. Here, we study quasicrystals described by the geometric cut-and-project method [15]. The aim is to show that tiling spaces associated with quasicrystals exhibit anyonic behavior, which can lead to TQC implementations. More specifically, we aim to establish lower-dimensional quasicrystals as a new candidate to implement TQC.

Although crystallographic materials have well-developed theories, mainly Bloch and Floquet's theories, these theories do not work properly for the topological aspects of quasicrystals due to the lack of translational symmetry [16]. Nevertheless, the connection between lower-dimensional quasicrystals with higher-dimensional lattices allows us to adapt and to use aspects of the known crystallographic theories considering the subspaces of the higher-dimensional Hilbert spaces. The physics of aperiodic order is a growing and active field of research [16–32]. Topological superconductors have been investigated in quasicrystals, suggesting that they can exhibit topological phases of matter [33–43].

We present a connection between anyons and one- and two-dimensional quasicrystals, such as the 5-fold Penrose tiling, by the isomorphism between the anyonic fusion Hilbert space and the subspaces of lattices Hilbert spaces describing quasicrystal tiling spaces. Both spaces have dimensions that grow with the Fibonacci sequence. A theorem from functional analysis says that two Hilbert spaces are isomorphic if, and only if, they have the same dimensions. We propose that these subspaces are fusion Hilbert spaces and show an isomorphism between the Fibonacci C^*-algebra of Fibonacci anyons and a C^*-algebra associated with the tiling spaces of quasicrystals. The C^*-algebra of interest allows for the implementation of representations of the braid group necessary for topological quantum computing. It is worth mentioning that, within the Bloch theory for periodic atomic structures, the energy level quantization maps to the periodic point group symmetry. As with similar approaches that go beyond the periodic structures, e.g., [44], quasicrystal approaches make use of this by restricting to subspaces of the crystalline structures.

This paper is organized as follows: in Section 2, we review and discuss elements of anyonic fusion Hilbert spaces and the Fibonacci C^*-algebras to establish the correspondence with the tiling spaces of quasicrystals. In Section 3, we discuss aspects of information processing in tiling spaces. We present discussions and implications in Section 4.

2. Correspondence between Anyons and Quasicrystals

The quintessential and simplest non-abelian anyon is the Fibonacci anyon [8,9]. We will show the isomorphism between anyonic fusion Hilbert spaces and quasicrystalline Hilbert spaces at the level of the Fibonacci anyons and Fibonacci quasicrystals, namely the one-dimensional Fibonacci chain and the 5-fold two-dimensional Penrose tiling. The name Fibonacci in Fibonacci anyons is due the dimensions of their Hilbert spaces being a well-known Fibonacci number, and, in the case of the mentioned quasicrystals, we will show that they have the same behavior, justifying the name Fibonacci.

2.1. Fibonacci Anyons and Fibonacci C^*-Algebra

There are different ways to describe anyons, including the Chern–Simons (CS) theory and lattice Hamiltonian approach [8,9]. For CS theory, it is well known that there is an additional gauge-invariant term that can be added to the Maxwell or Yang–Mills Lagrangian in (2 + 1) dimensions. This CS term is topological, as it does not depend on the metric [8,45]. At low temperatures, this term dominates. In the non-abelian case, the action is invariant under SU(2) $\cong$ Spin(3) and can be written as a Gauss constraint on a wave function of the gauge fields.

In the presence of sources (representations of a Lie algebra), anyonic behavior, such as fusion and braid dynamics, can be found with sufficient control of the low-temperature Hamiltonian, Lagrangian, or Gaussian constraints. The degenerate ground state of the effective theory is associated with the CS sources form the so-called fusion Hilbert space, which is proposed as a fault-tolerant topological quantum computing substrate. In the case of Fibonacci anyons, the sources can only be in the two lower-dimensional representations of SO(3), the spin-0 and spin-1 representations, with the fusion rules

$$1 \otimes 1 = 0 \oplus 1$$
$$0 \otimes 1 = 1$$
$$1 \otimes 0 = 1. \tag{1}$$

If we have N spin-1 representations as sources and start to fuse them, they can build different fusion paths that can lead to either spin-1 or spin-0 representations with certain probabilities. The different paths to fuse the N spin-1 sources to only one spin-1 or spin-0 source can be seen as states in a fusion Hilbert space H_N, where its dimension grows with the number of original spin-1 sources and is given by the Fibonacci sequence, $((0, 1,)1, 2, 3, 5, 8, 13, \ldots, Fib(N+1))$ [46], i.e., $H_N = \mathbb{C}^{Fib(N+1)}$, where $Fib(N+1)$ is the $N+1$th Fibonacci number.

Rotating one physical source around the other is equivalent to an operation in the fusion Hilbert space described by the so-called braid operators (higher-dimensional representations of the braid group), which leads to non-trivial statistics given the necessary quantum evolution for topological quantum computation. The explicit construction of braid operators, B, is given as examples in ([46], Sections 2.4 and 2.5) through the so-called F-matrices and R-matrices operating in the fusion Hilbert space. For the case of fusing two anyons into a third one, this process is a five-dimensional space, and the explicit matrices in a suitable base can be given by

$$R = diag(e^{4\pi i/5}, e^{-3\pi i/5}, e^{-3\pi i/5}, e^{4\pi i/5}, e^{-3\pi i/5}),$$

$$F = \begin{bmatrix} 1 & & & & \\ & 1 & & & \\ & & 1 & & \\ & & & \phi^{-1} & \phi^{-1/2} \\ & & & \phi^{-1/2} & -\phi^{-1} \end{bmatrix}, \tag{2}$$

with $B = FRF^{-1}$ and $\phi = 2\cos(\frac{\pi}{5}) \approx 1.618$, the golden ratio.

More details on Fibonacci anyons are well known and can be found in Ref. [46] and references therein. Less known is the isomorphism of the fusion Hilbert spaces with representations of certain C^*-algebras, in particular, the so-called Fibonacci C^*-algebra [12]. In [12], it is shown that the fusion rules determine the data of a Bratteli diagram [47], which specifies an approximately finite-dimensional (AF) C^*-algebra with a representation on a Hilbert space, which is isomorphic to the anyonic fusion Hilbert space. An AF C^*-algebra $\mathcal{A}$ is given by a direct limit $\mathcal{A} = \varinjlim \mathcal{A}_n$ of a finite-dimensional C^*-algebra $\mathcal{A}_n$, where $\mathcal{A}_n$ is a direct sum of matrix algebras over $\mathbb{C}$, $\mathcal{A}_n = \oplus_{k=1}^{N_n} \mathcal{M}_{r_k}(\mathbb{C})$. Similarly, a Hilbert-space representation of $\mathcal{A}$, $H^{\mathcal{A}}$, is obtained as a direct limit of a system of finite-dimensional Hilbert spaces $H_n^{\mathcal{A}}$, $H_n^{\mathcal{A}} = \oplus_{k=1}^{N_n} \mathbb{C}^{r_k}$. A Bratteli diagram yields a unique C^*-algebra and allows for a simpler computation of the dimension of the Hilbert-space representations of this algebra by counting the number of paths to a certain node. For the Fibonacci C^*-algebra, see ([48], Example III.2.6) and ([12], Section 3.2), for the Bratteli diagram illustration and the dimension of the Hilbert-space computation. The isomorphism between the representations of Hilbert spaces and the anyonic-fusion Hilbert spaces is given in ([12], Lemma 3.3), where the dimensions of Fibonacci anyons and the Fibonacci C^*-algebra both grow with the Fibonacci sequence.

2.2. Fibonacci Quasicrystals and the Fibonacci C*-Algebra

In analogy with the anyonic case, we will provide a physical description of the anyonic behavior of quasicrystals to allow for concrete physical implementation and then the associated effective fusion Hilbert space to deal with topological quantum information processing. It is more common to deal with quasicrystals from the point of view of Bloch theory for periodic many-body atomic quantum systems, but even within this point of view there are different implementations. While the quasicrystal literature is fast growing, we mention the quasicrystalline extension of the Bloch theory in context of the gap-labelling theorem [16] and the discovery of a few exact solutions for quasicrystal Hamiltonians [17–19,25,28,32]. We also highlight more developments in terms of computations of the spectrum and band structure [20–24,26,27] and the study of topological properties [33–39]. Finally, quasicrystals have been actively studied in recent years [29–31,40–43,49]. From our understanding, the different approaches have convergent results, including the self-similar structure of the energy spectrum, band structure, and topological protected phases. The geometric cut-and-project method, or its more general form, called model sets, describes this structure.

The starting point is the periodic Bloch theory considering the Schrodinger equation for a particle over the atomic structure with a periodic potential $V(r + R) = V(r)$ for all lattice vectors R of a given lattice $\mathcal{L}$. With this setup, the Hamiltonian commutes with the translation operators, and the Bloch theory diagonalizes both simultaneously. For this, one introduces the reciprocal lattice $\mathcal{L}^*$ with primitive translation vectors K, where the scalar product $R \cdot K$ is an integer multiple of 2π. The eigenfunctions are such that k exists as

$$\psi_{k+K}(r + R) = e^{ik \cdot R} \psi_k(r), \tag{3}$$

in which $\psi_k(r)$ the Bloch wavefunctions on $\mathbb{R}^n \times \mathbb{R}^n$ (r in the Voronoi cell V and k in its dual V^*, also called Brillouin zone). The curves of the spectrum are periodic in a dual reciprocal space, and the entire band structure is defined by the band structure inside the first Brillouin zone.

Our idea is to study the Hilbert space of ψ's satisfying Bloch's theorem, such that $||\psi||^2 < \infty$. We then introduce, for each $k \in V^*$, the Hilbert space H_k of the functions u on $\mathbb{R}^n$, such that

$$u(r + R) = e^{ik \cdot R} u(r), \tag{4}$$

and $||u||^2 < \infty$, with $H^{\mathcal{L}} = \oplus H_k$, and the dimension grows with the number of points on the lattice. The Hilbert spaces for a particle over an aperiodic potential from a quasicrystal will be seen as a subspace of the lattice Hilbert space $H^{\mathcal{L}}$, and we will need to review the cut-and-project method to obtain the quasicrystal from the lattice $\mathcal{L}$.

We consider a cut-and-project scheme (CPS) to be a 3-tuplet $\mathcal{G} = \left(\mathbb{R}^d, \mathbb{R}^{d'}, \mathcal{L} \right)$, where the parallel space $\mathbb{R}^d$ and the perpendicular space $\mathbb{R}^{d'}$ are real euclidean spaces, $\mathcal{L}$ is the lattice in $\mathcal{E} = \mathbb{R}^d \times \mathbb{R}^{d'}$, and is the embedding space with two natural projections π: $\mathbb{R}^d \times \mathbb{R}^{d'} \to \mathbb{R}^d$ and $\pi_\perp$: $\mathbb{R}^d \times \mathbb{R}^{d'} \to \mathbb{R}^{d'}$ subject to the conditions that $\pi(\mathcal{L})$ is injective, and that $\pi_\perp(\mathcal{L})$ is dense in $\mathbb{R}^{d'}$. With $L = \pi(\mathcal{L})$, this scheme has a well-defined map called the star map $\star : L \to \mathbb{R}^{d'}$:

$$x \longmapsto x^\star := \pi_\perp(\pi^{-1}(x)). \tag{5}$$

For a given CPS $\mathcal{G}$ and a window W, quasicrystal point sets $(\triangle_\gamma^\lambda(W))$ can be generated by setting two additional parameters: a shift $\gamma \in \mathbb{R}^d \times \mathbb{R}^{d'}/\mathcal{L}$ with $\gamma_\perp = \pi_\perp(\gamma)$ and a scale parameter $\lambda \in \mathbb{R}$. The projected set

$$\triangle_\gamma^\lambda(W) := \{x \in L \mid x^\star \in \lambda W + \gamma_\perp\} = \{\pi(y) \mid y \in \mathcal{L}, \pi_\perp(y) \in \lambda W + \gamma_\perp\}, \tag{6}$$

gives the quasicrystal point set.

Another important concept is the tiling of the Euclidean space from the point set. Consider that a pattern $\mathcal{T}$ in $\mathbb{R}^d$ ($\mathcal{T} \sqsubset \mathbb{R}^d$) is a non-empty set of non-empty subsets of $\mathbb{R}^d$. The elements of $\mathcal{T}$ are the fragments of the pattern $\mathcal{T}$. A tiling in $\mathbb{R}^d$ is a pattern

$\mathcal{T} = \{T_i \mid i \in I\} \sqsubset \mathbb{R}^d$, where I is a countable index set, and the fragments T_i of $\mathcal{T}$ are non-empty closed sets in $\mathbb{R}^d$ subject to the conditions

1. $\cup_{i \in I} T_i = \mathbb{R}^d$,
2. $int(T_i) \cap int(T_j) = \varnothing$ for all $i \neq j$, and
3. T_i is compact and equal to the closure of its interior $T_i = \overline{int(T_i)}$.

While this is trivial for lattices with unique unit cells, quasicrystals have more than one unit cell. Multiple quasicrystals with the same number of points N from $\mathcal{L}$ projected to the parallel space can lead to different tilings depending on the shift parameter γ.

The construction above identifies the quasicrystal point set as a subset of the original lattice in the embedding space and its Hilbert space $H^{\triangle}$ as a subspace of the lattice Hilbert space $H^{\mathcal{L}}$. An explicit example is given in ([16], Section 3.2) for the one-dimensional Fibonacci chain derived from the $\mathbb{Z}^2$ lattice. This provides access to the physical properties of quasicrystals, such as their electronic structure. However, the full tiling structure is not properly captured by these descriptions. To address the different tiling configurations of quasicrystals, it is standard to consider the associated C^*-algebra structures ([50], Sections II.3 and V.10) and the notion of tiling spaces [51]. A simple way to look at this is to decompose the quasicrystalline Hilbert space $H^{\triangle}$ further according to tile configurations. The one-dimensional Fibonacci chain and the two-dimensional Penrose tiling can be described by only two tiles. For the Fibonacci chain, they are called long (L) and short (S) edges. For the Penrose tiling, they can be given either by a fat rhombus (F) and a thin rhombus (T) or two quadrilaterals called kites and darts.

We can then consider the Hilbert spaces $H^{\triangle}_{L,F}$ and $H^{\triangle}_{S,T}$ associated with the two different tiles. The frequency of the appearance of these tiles in some tiling is constant and grows with the Fibonacci sequence, given, at some step, as $F(N)$ for L or F to $F(N-1)$ for S or T. From the Bloch theory, the number of states depends on the number of points in the lattice, which translates to the number of tiles. A lattice trivially has only one tile. For quasicrystals, the number grows differently depending on the tiling considered. Both the Fibonacci chain and the Penrose tiling contain two fundamental tiles that grow with the Fibonacci sequence. As such, the Hilbert spaces $H^{\triangle}_{L,F}$ and $H^{\triangle}_{S,T}$ subspaces of a quasicrystalline Hilbert space (which are subspaces of lattices Hilbert spaces) have dimensions that grow with the number of tiles added to the quasicrystal in the same way that the dimensions of the anyonic fusion Hilbert spaces grow with the addition of anyons. Following the discussion from the previous section, we conclude that these quasicrystalline subspaces are candidates for the implementation of representations of the Fibonacci C^*-algebra associated with Fibonacci anyons. We see the tiles emerging from the Bloch theory playing the same role of the non-abelian $SO(3)$ sources in the Chern–Simons theory.

Another perspective is to consider the tiling space, which leads to Hilbert spaces that are isomorphic to the ones considered above with dimensions growing with the Fibonacci sequence. Basically, we start with a quasicrystal point set $\triangle_\gamma$ and associates a tiling with it. Then, we can shift the point set by shifting the window in perpendicular space using $\gamma_\perp$. Each shift generates a new tiling with the same tiles but with a different configuration, where these tiles can be seen in both parallel and perpendicular spaces due to the star map. The difference is that, in parallel space, there is a growth of the quasicrystal with tiles of fixed length, while, in the perpendicular space, each point added rescales the tiles and reorganizes the configuration leading to a rescaling of the space, which is usually called *inflation* or *deflation* for the inverse process. Each tiling is a point in the so-called tiling space, which encodes all possible tilings that can be made with a fixed CPS and window. To encode this information, we can fix a point x inside the window in the perpendicular space. As the points are projected, with $\pi_\perp(\mathcal{L})$, we can track the tile type around x after a new point is projected. Then, we can generate different tilings from different shifts and track the sequence of tiles around that point x over the different sequence of projections.

Equivalently, one can use only one projection and track the evolution of different positions inside the window. Each tiling is described by a sequence that encodes the

evolution of tiles around x in the perpendicular space as the quasicrystals grow in parallel space. By labelling the Fibonacci-chain and Penrose-tiling letters L or F as the symbols 1, and S or T as 0 we can associate different sequences $(x_i)_n$ of 0s and 1s with x, where i indexes the different sequences of projections, and $n \in \mathbb{N}$ is the level in one sequence of projections. The only constraint on these sequences, which arises from the geometry of the CPS with fixed window, is that, if $(x_i)_n = 0$, then $(x_i)_{n+1} = 1$. We illustrate this for the Fibonacci chain in Figure 1, where $x_1 = 1111101\ldots$, and $x_2 = 011011\ldots$, for example.
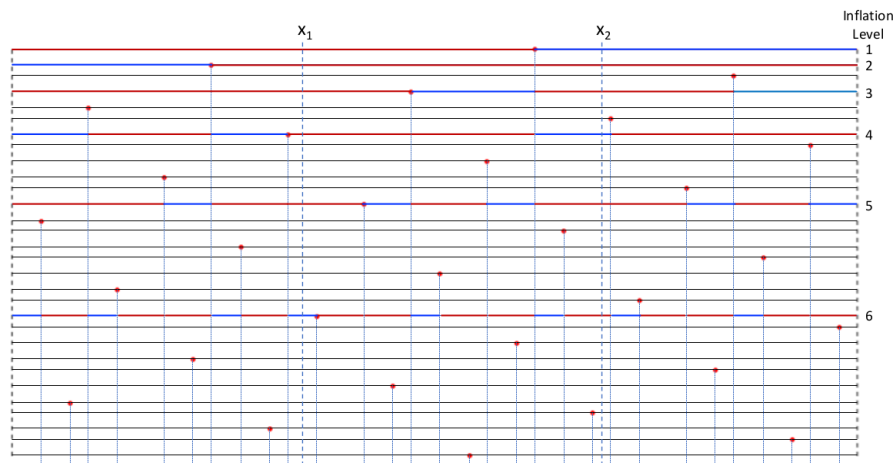
Figure 1. The segment of the window in perpendicular space for the Fibonacci chain is shown at each inflation/deflation level. The L tiles are in red and S tiles in blue. On the horizontal axis, we show specific Fibonacci-chain configurations, where the number of tiles grows with the Fibonacci sequence. The sequences $(x_i)_n$ are given by vertical lines. For example, we show two possible sequences at x_1 and x_2.

The Penrose tiling is shown in Figure 2, where $x_1 = 110\ldots$, and $x_2 = 111\ldots$

Additionally, an equivalence relation is defined on this space of sequences. Tilings T_i and T_j with some m, such that $(x_i)_n = (x_j)_n$ for $n \geq m$, are equivalent. This is presented in detail in ([50], Sections II.3 and V.10) for the tiling space of the Penrose tiling with the construction of a C^*-algebra $\mathcal{A}$ associated with this space. Remarkably, this algebra is the same Fibonacci C^*-algebra; the Hilbert-space representations are isomorphic to the anyonic fusion Hilbert spaces [12]. In the next section, we present detailed aspects of this algebra, quasicrystal physics interpretations, and topological quantum computation.

Let us consider a concrete solution of a Hamiltonian for a quasicrystal. Despite the difficulties with the generalization of the Bloch's and Floquet's theories, there are a few known exact solutions for quasicrystal Hamiltonians. Some of the state solutions of the so-called tight-binding model for the Fibonacci chain and the Penrose tiling are known [17–19,25,28,32]. These states include zero-energy degenerate states and have a similar form to the Bloch wave function, Equation (4), given by

$$\psi(i) = C(i)e^{\kappa h(i)} \tag{7}$$

where $\kappa \in \mathbb{R}$ is a constant, $C(i)$ are local site-dependent periodic functions given the local amplitudes and $h(i)$ is a non-local height field dependent on the geometry of the specific tiling. For the Fibonacci chain in Equation (7), the zero-energy state takes the form $\psi(2i) = (-1)^i e^{\kappa h(2i)}$ with $\kappa = \ln \phi$, and the field $h(2i)$ given by

$$h(i) = \sum_{0 \leq j \leq i} B(2j \to 2(j+1)), \tag{8}$$

where $B(LS) = 1$, $B(SL) = -1$, and $B(LL) = 0$. For the Penrose tiling, both κ and $C(i)$ are computed numerically [28], but the ribbon description discussed above allows us to access

the Fibonacci chain subspaces directly. Note that a flip $LS \rightarrow SL$, such as the the the one for the ribbon R_b in Figure 3, changes the state by a factor of ϕ^{-2}, $\psi^{LS}(i) = \phi^{-2}\psi^{SL}(i)$.
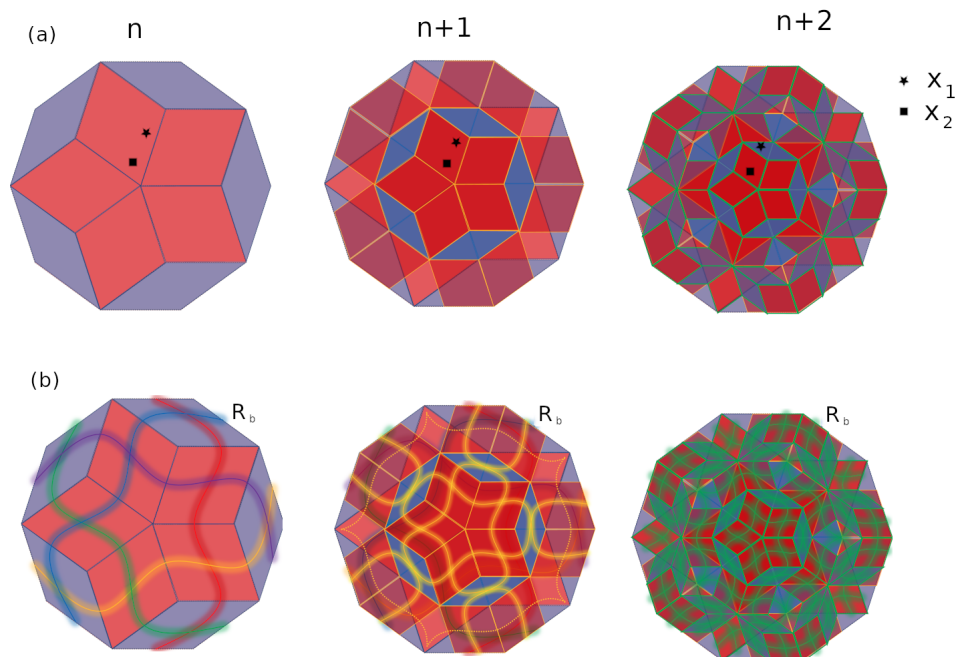
Figure 2. In (**a**), we show three inflations tracking two positions $x_1 = 110$ and $x_2 = 111$ over the inflation levels with the fat rhombus in red and the thin in blue. In (**b**), we introduce the ribbon description. The ribbons are constructed by straight lines (smooth for illustration purposes on the image) going from the center of one tile to the center of an adjacent tile following the Fibonacci rules on the same level as the inflations. For example, the ribbon R_b (the blue in the nth level) goes over the following tiles in the three levels shown: TFFT, FTFFTF and FTFTFFTFTF. Note that a ribbon going over an F in one level will go over an F and T in the next inflation level, and a ribbon going over an S will always go to an F.
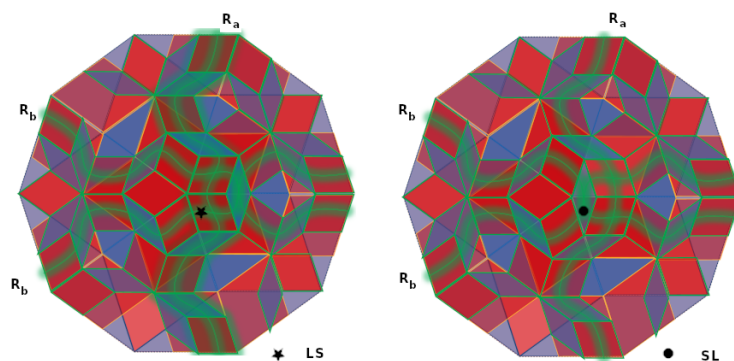
Figure 3. A tile flip that sends ribbons R_b from FTFTF**FT**FTF to FTFTF**TF**FTF given a factor of ϕ^{-2} on the associated states. The Ribbon R_a has a change in orientation on the flip position.

3. Quasicrystalline Topological Quantum Information Processing

Following the Bloch theory, a quantum–mechanical quasicrystal is described by a Hilbert space, which is a subspace of a Hilbert space describing a higher-dimensional crystal (the lattice $\mathcal{L}$ from the previous section). In principle, this gives us a mechanism to grow a quasicrystal while maintaining the quantum superposition of tilings in a tiling space. This growth is described by the sequences of 0s and 1s (encoding the different two tiles in the Fibonacci chain or Penrose tiling) $(x_i)_n$, such that, if $(x_i)_n = 0$, then $(x_i)_{n+1} = 1$ and is subject to some equivalence relation, such as the one described in the previous

section with one associated algebra $\mathcal{A}$. A slightly different, but equivalent way to address the tiling space is to consider finite sequences $(x_i)_n$, $n = 1, \ldots, N$ subject to the same rule and, with a equivalence relation given by $(x_i)_N = (x_j)_N$, construct the algebra $\mathcal{A}$ as the inductive limit of finite-dimensional algebras $\mathcal{A}_N$ with $\mathcal{A}_N$ as a direct sum of the matrix algebras [52]. For the Fibonacci chain and Penrose tiling described by just two tiles, the set of equivalence classes has only two elements, with the number of both tiles growing with the Fibonacci sequence (for example L grows with $F(N + 1)$ and S with $F(N)$), which gives $\mathcal{A}_N = M_{d_L^n} \oplus M_{d_S^n}$ with $d_l^n = F(N + 1)$ and $d_S^n = F(N)$. The embedding of $\mathcal{A}_N$ in $\mathcal{A}_{N+1}$ is given by $d_L^{n+1} = d_L^n + d_S^n$ and $d_S^{n+1} = d_L^n$. To conduct the inverse process and merge tiles, one can define a projection at the step N by means of the operation to forget that step, remaining with sequences with $n = 1, \ldots, N - 1$.

One can then consider projections E_n acting on the associated Hilbert spaces defined by $\mathcal{A}_N$, such that E_n maps the Hilbert space $H_{d_L^n}$ to $H_{d_L^{n-1}}$ or subspaces of $H_{d_L^n}$ associated with $\mathcal{A}_N$ with the subspaces of $H_{d_L^{n-1}}$ associated with $\mathcal{A}_{N-1}$ [53]. Following ([50], Lemma 5 in section V.10), we consider a sequence of E_n orthogonal projections, known as Jones–Wenzl projections, such that the following relations hold

$$
\begin{align}
E_n^2 &= E_n \tag{9} \\
E_n E_m E_n &= \phi^{-2} E_n, \quad \text{if } |n - m| = 1 \tag{10} \\
E_n E_m &= E_m E_n, \quad \text{if } |n - m| > 1, \tag{11}
\end{align}
$$

where, for more general quasicrystals, one could consider Equation (10) to be $E_n E_m E_n = [2]_q^{-2} E_n$, with the so-called quantum numbers $[n]_q$ given by

$$
[n]_q = \frac{q^n - q^{-n}}{q - q^{-1}} \tag{12}
$$

with $q = e^{\frac{\pi i}{r}}$. In the case of Equations (9)–(11), we have q, a fifth root of unity, $r = 5$, and we call the algebra $\mathcal{A}_N(q)$.

In the study of Fibonacci anyons, the Temperley–Lieb algebra with generators F_n is typically used, such that $E_n = \phi^{-1} F_n$, see ([8], Section 8.2.2) and [54]. The algebra defined by the projections E_n, Equations (9)–(11), is isomorphic to the Fibonacci C^*-algebra of the Fibonacci anyons and Fibonacci quasicrystals, the proof can be seen by explicitly deriving its Bratteli diagram [53]. The quasicrystal projections can be used to implement the braid operations necessary for quantum evolution to implement topological quantum computing. In the case of anyons, moving one anyon around the other is a non-trivial operation encoded in the braid group operations on the fusion Hilbert space. For non-abelian anyons, these operations are shown to be dense in $SU(N)$, with N as the number of anyons in the system to provide universal quantum computation. The braid group is generated by generators B_n satisfying the relations

$$
\begin{align}
B_n B_n^{-1} &= B_n^{-1} B_n, \\
B_n B_m B_n &= B_m B_n B_m, \quad \text{if } |n - m| = 1 \\
B_n B_m &= B_m B_n, \quad \text{if } |n - m| > 1. \tag{13}
\end{align}
$$

A representation of the braid group can be given from the algebra in Equation (11) by

$$
\begin{align}
\rho_A(B_n) &= \phi A E_n + A^{-1} \mathbb{I} \\
\rho_A(B_n^{-1}) &= \phi A^{-1} E_n + A \mathbb{I}, \tag{14}
\end{align}
$$

with $\phi = -A^2 - A^{-2}$, where unitarity is guaranteed if the projections E_n are Hermitian. A contains four solutions, all with $|A| = 1$. The four solutions are $A = e^{3\pi i/5}$, $-e^{3\pi i/5}$, $e^{2\pi i/5}$,

and $-e^{2\pi i/5}$. Note that the R-matrix for Fibonacci anyons in Equation (2) contains $e^{3\pi i/5}$ on some of the diagonals. With the solution of A provided, one can verify that

$$
\begin{aligned}
\rho_A(B_n)\rho_A(B_n^{-1}) &= \rho_A(B_n^{-1})\rho_A(B_n) & \\
\rho_A(B_n)\rho_A(B_m)\rho_A(B_n) &= \rho_A(B_m)\rho_A(B_n)\rho_A(B_m) & \text{if } |n-m| = 1 \\
\rho_A(B_n)\rho_A(B_m) &= \rho_A(B_m)\rho_A(B_n) & \text{if } |n-m| > 1.
\end{aligned}
\tag{15}
$$

Therefore, the quasicrystal projection operators can be used to construct a representation of the braid group.

The usual step from quantum computation to topological quantum computation can now be performed with quasicrystals by finding an embedding $\mathfrak{e}$ of an N-qubit space $(\mathbb{C}^2)^{\otimes N}$ into a subspace of the tiling space. The embedding does not need to be efficient, because it is well known that the braid group can approximate any universal quantum gate to any desired precision. The computational subspace of the tiling space can be given by fixing one equivalence class $(x_i)_n$, $n = 1, \dots, 2N+1$ and $i = 1, \dots, d$ with d the number of sequences with $(x_i)_{2N+1} = 1$. We represent this subspace using $T_{N,1} = (x_i)_n$. Finally, to simulate a quantum circuit, we can have

$$
\begin{array}{ccc}
\left(\mathbb{C}^2\right)^{\otimes N} & \xrightarrow{\mathfrak{e}} & T_{N,1} \\
U \downarrow & & \downarrow \rho_A(B) \\
\left(\mathbb{C}^2\right)^{\otimes N} & \xrightarrow{\mathfrak{e}} & T_{N,1}.
\end{array}
\tag{16}
$$

Explicit matrix representations of $\rho_A(B)$ can be obtained from the algebra $\mathcal{A}_N(q)$ acting on the N-qubit Hilbert space $(\mathbb{C}^2)^{\otimes N}$, a subspace of the tiling space. Define $E(q)$ acting on $\mathbb{C}^2 \otimes \mathbb{C}^2$ as [55]

$$
E(q) = [2]_q^{-1}\left(q^{-1}e_{11} \otimes e_{22} + q e_{22} \otimes e_{11} + e_{12} \otimes e_{21} + e_{21} \otimes e_{12}\right)
\tag{17}
$$

with e_{ij} the two-dimensional matrix units and $E_i(q) = \mathbb{I} \otimes \dots \otimes \mathbb{I} \otimes E(q) \otimes \dots \otimes \mathbb{I}$, where $E(q)$ acts on the positions i and $i+1$ of the tensor product.

For TQC with a quantum–mechanical quasicrystal, suppose that researchers in the future could have complete control of how the quasicrystal is inflated or deflated. The number of possible inflation/deflation paths in the tiling space, which gives the Hilbert-space dimension, is tied to the number of physical tiles, analogous to how the number of physical anyons define the fusion Hilbert-space dimension. This allows us to obtain a dictionary between concepts related to Fibonacci anyons and TQC with a quantum-mechanical quasicrystal. For concreteness and simplicity, consider the Fibonacci chain, which has two inflation rules

$$
\begin{array}{ll}
\text{Rule A:} & \{\text{L} \to \text{LS, S} \to \text{L}\} \\
\text{Rule B:} & \{\text{L} \to \text{SL, S} \to \text{L}\}.
\end{array}
\tag{18}
$$

To clarify, our conventions are that the inflation rules apply an inflation. It can be verified that the successive application of Rule A seeded by S leads to the reverse of the chain found by the successive application of Rule B. If n arbitrary combinations of Rule A and Rule B are applied from the seed, then 2^n states can be found. However, these lead to various duplicate tilings, such that $Fib(n+2)$ unique tilings are found. For example, with seed L, for $n = 2$ we have {{L, SL, LSL}, {L, SL, LLS}, {L, LS, SLL}, and {L, LS, LSL}} resulting in three unique states {LSL, LLS, SLL}, or, in terms of the (x_i), $i = 1, 2, 3$, describing the associated tiling space, we have {LSL, LLS, LLL}. The associated Bratteli diagram is shown in Figure 4, which is equivalent to the Fibonacci anyon diagram [12] and the $\mathcal{A}_N(q)$ diagram for the Jones–Wenzl projections [53].
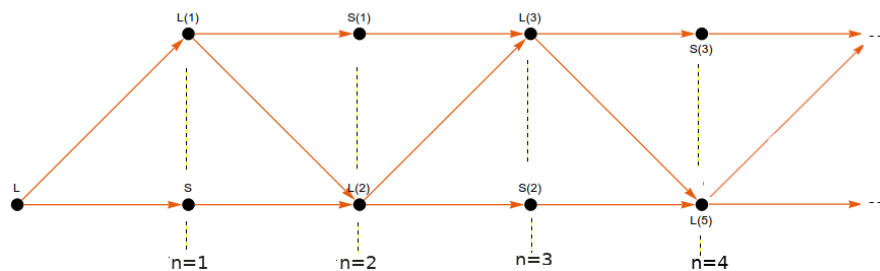
Figure 4. A Bratteli diagram for the Fibonacci chain (similar for the Penrose tiling with fat (F) and thin (T) rhombus), where each path, i, to a node gives a x_i, and the different inflation levels n are shown. The number in parentheses is the number of paths to that node at level N, $n = 1, \ldots, N$, which gives the Hilbert-space dimension for the associated subspace with sequences $(x_i)_N = L$ or S.

The analogue of an anyonic fusion process is given by the operation to forget the Nth step in $(x_i)_n$, $n = 1, \ldots, N$, leaving the sequences $(x_i)_n$ with $n = 1, \ldots, N - 1$. This sends the system from level N to $N - 1$ or the Hilbert space of dimension from $F(n)$ to $F(n - 1)$ and is equivalent to a deflation of the physical quasicrystal. Since L is a fixed length, this operation acting on the Hilbert space associated with the two tiles LS would lead to L as a deflation, which decreases the length of the chain. When performing the analogue of braiding in the quasicrystal, one specifies a basis given by inflation/deflation paths $(x_i)_n$ and decomposes the projection E_n in a direct sum of projections acting in lower-dimensional subspaces. From Equation (14), the subspace acted in by E_n reaches a different phase, which relates to A and a rescaling by ϕ. In usual anyonic systems, the braid operations involve a basis transformation. This selects two anyons to be fused and applies an operation to these two anyons, which gives a phase R and then applies an inverse basis transformation. In quasicrystals, the projection E_n directly selects the subspace to be acted on by a phase and rescaling. Table 1 summarizes a dictionary that compares the aspects of Fibonacci anyons and quantum–mechanical Fibonacci chains for TQC.

Table 1. A dictionary comparing concepts related to Fibonacci anyons and TQC with a quantum–mechanical Fibonacci chain is provided.

Fibonacci Anyons	Quantum Fibonacci Chain
Anyon	Tile
0, 1	S, L
d-fold degeneracy	# of tiles
Fusion with 1 (anyon destruction)	Deflation (tiles merging)
Braid $B = FRF^{-1}$	$\rho_A(B_n) = A\phi E_n + A^{-1}\mathbb{I}$

We have already noted that crystallographic theories, mainly Bloch's and Floquet's theories, do not extend directly to quasicrystals due to the lack of translational symmetry. We also discussed an isomorphism between anyonic and quasicrystalline Hilbert spaces. In this context, it is tempting to import well-developed techniques from anyonic systems for applications in quasicrystals to implement TQC. One example is the so-called golden chain [56], which models Fibonacci anyons in one dimension. The golden chain has a natural realization in terms of the Fibonacci-chain quasicrystal. The local Hamiltonian H_i acting on the ith Fibonacci anyon on the chain discussed in [56] is immediately identified with the projections E_n, acting on the inflation level n, $(x)_n$ of the Fibonacci-chain quasicrystal, allowing access to the quantum quasicrystal growth and shrinkage. A detailed analysis of this Hamiltonian (and other anyonic Hamiltonians) in the context of quasicrystals and their relationship with quasicrystal Hamiltonians could be discussed in future work.

4. Implications

Conceptually, topological quantum computing is known to have advantages over standard quantum computing for scaling due to hardware-level error protection. However, the physical implementation of topological phases of matter is a big challenge. One main line of research is to implement localized Majorana modes, which can behave as abelian Ising anyons. This line of research has seen a major setback recently, with a main group of researchers withdrawing papers that claimed experimental validation of abelian anyons, in particular the Majorana fermion excitations [57,58]. Additionally, non-abelian anyons need to be discovered to implement anyonic TQC. This opens the opportunity for new approaches to topological quantum computing through the discovery of new hardware platforms that can support the anyonic quantum information processing.

In this work, we investigated lower-dimensional quasicrystals as a platform for TQC. In summary, we showed that quasicrystals exhibit anyonic behavior and that its tiling spaces can encode topological quantum information processing. Consider two key ingredients. First, note that the fusion Hilbert-space representations of the C^*-algebras associated with anyonic systems possess a growing dimension equal to the tiling Hilbert spaces of quasicrystals, which can be demonstrated through Bratteli diagram constructions. Second, topological quantum information can be processed by finding a suitable computational subspace of the tiling spaces where the necessary operations such as the braid group transformations can be implemented, for example, using the explicit representations of the projection's Equation (17). A dictionary comparing information processing with Fibonacci anyons and quantum-mechanical Fibonacci chain was provided in Table 1.

The novelty of our work is the proposal of quasicrystal materials as a natural platform for topological quantum computing. These materials exhibit aperiodic and topological order, and they are already implemented in laboratories around the world. More difficult is the manipulation of the topological properties of tiling spaces of quasicrystals required for the task of quantum information processing, to which our work adds further theoretical understanding. A complete proposal for concrete experimental implementation remains an open problem. One idea is to use graphene etching with an inner quasicrystal layer to create the circuit connections, where inflation could be implemented by disconnecting a lot of connections along the chain in line with recent advances in the field [59–62].

Author Contributions: Conceptualization, M.A. and K.I.; methodology, M.A.; software, M.A., D.C. and F.F.; validation, D.C. and F.F.; formal analysis, M.A.; investigation, M.A., D.C.; writing—original draft preparation, M.A.; writing—review and editing, M.A. and D.C.; visualization, D.C.; supervision, M.A. and K.I.; funding acquisition, K.I. All authors have read and agreed to the published version of the manuscript.

Institutional Review Board Statement: Not applicable.

Informed Consent Statement: Not applicable.

Data Availability Statement: Not applicable.

Conflicts of Interest: The authors declare no conflict of interest.

References

1. Nielsen, M.A.; Chuang, I.L. *Quantum Computation and Quantum Information*, 10th Anniversary ed.; Cambridge University Press: Cambridge, UK, 2011.
2. Barbara, M.; Terhal, B.M. Quantum error correction for quantum memories. *Rev. Mod. Phys.* **2015**, *87*, 307. [CrossRef]
3. Kelly, J.; Barends, R.; Fowler, A.G.; Megrant, A.; Jeffrey, E.; White, T.C.; Sank, D.; Mutus, J.Y.; Campbell, B.; Chen, Y.; et al. State preservation by repetitive error detection in a superconducting quantum circuit. *Nature* **2015**, *519*, 66–69. [CrossRef] [PubMed]
4. Djordjevic, I.B. *Quantum Information Processing, Quantum Computing, and Quantum Error Correction: An Engineering Approach*; Academic Press: Cambridge, MA, USA; Elsevier: Amsterdam, The Netherlands, 2021.
5. Seedhouse, A.E.; Hansen, I.; Laucht, A.; Yang, C.H.; Dzurak, A.S.; Saraiva, A. Quantum computation protocol for dressed spins in a global field. *Phys. Rev. B* **2021**, *104*, 235411. [CrossRef]

6. Breuckmann, N.P.; Eberhardt, J.N. Quantum Low-Density Parity-Check Codes. *PRX Quantum* **2021**, *2*, 040101. [CrossRef]
7. Wang, D.S. A comparative study of universal quantum computing models: Toward a physical unification. *Quantum Eng.* **2021**, *3*, e85. [CrossRef]
8. Pachos, J.K. *Introduction to Topological Quantum Computation*; Cambridge University Press: Cambridge, UK, 2012.
9. Wang, Z. *Topological Quantum Computation*; Number 112; American Mathematical Society: Providence, RI, USA, 2010.
10. Bartolomei, H.; Kumar, M.; Bisognin, R.; Marguerite, A.; Berroir, J.M.; Bocquillon, E.; Placais, B.; Cavanna, A.; Dong, Q.; Gennser, U.; et al. Fractional statistics in anyon collisions. *Science* **2020**, *368*, 173–177. [CrossRef]
11. Ding, L.; Wang, H.; Wang, Y.; Wang, S. Based on Quantum Topological Stabilizer Color Code Morphism Neural Network Decoder. *Quantum Eng.* **2022**, *2022*, 9638108. [CrossRef]
12. Marcolli, M.; Napp, J. Quantum Computation and Real Multiplication. *Math. Comput. Sci.* **2015**, *9*, 63–84. [CrossRef]
13. Planat, M.; Aschheim, R.; Amaral, M.M.; Irwin, K. Universal quantum computing and three-manifolds. *Symmetry* **2018**, *10*, 773. [CrossRef]
14. Planat, M.; Amaral, M.M.; Fang, F.; Chester, D.; Aschheim, R.; Irwin, K. Character varieties and algebraic surfaces for the topology of quantum computing. *Symmetry* **2022**, *14*, 915. [CrossRef]
15. Baake, M.; Grimm, U. *Aperiodic Order*; Cambridge University Press: Cambridge, UK, 2013.
16. Bellissard, J. Gap labelling theorems for Schrödinger's operators. In *From Number Theory to Physics*; Luck, J.M., Moussa, P., Waldschmidt, M., Eds.; Les Houches March 89; Springer: Berlin/Heidelberg, Germany, 1992; pp. 538–630. [CrossRef]
17. Kohmoto, M.; Sutherland, B. Electronic States on a Penrose Lattice. *Phys. Rev. Lett.* **1986**, *56*, 2740. [CrossRef] [PubMed]
18. Sutherland, B. Self-similar ground-state wave function for electrons on a two-dimensional Penrose lattice. *Phys. Rev. B* **1986**, *34*, 3904. [CrossRef] [PubMed]
19. Fujiwara, T.; Kohmoto, M.; Tokihiro, T. Multifractal wave functions on a Fibonacci lattice. *Phys. Rev. B* **1989**, *40*, 7413(R). [CrossRef] [PubMed]
20. Luck, J.M. Cantor spectra and scaling of gap widths in deterministic aperiodic systems. *Phys. Rev. B* **1989**, *39*, 5834. [CrossRef]
21. Sütő, A. Singular continuous spectrum on a cantor set of zero Lebesgue measure for the Fibonacci Hamiltonian. *J. Stat. Phys.* **1989**, *56*, 525–531. [CrossRef]
22. Benza, V.G. Band spectrum of the octagonal quasicrystal: Finite measure gaps and chaos. *Phys. Rev. B Condens. Matter.* **1991**, *44*, 10343–10345. [CrossRef]
23. Kaliteevski, M.A.; Br, S.; Abram, R.A.; Krauss, T.F.; Rue, R.D.; Millar, P. Two-dimensional Penrose-tiled photonic quasicrystals: from diffraction pattern to band. *Nanotechnology* **2000**, *11*, 274. [CrossRef]
24. Florescu, M.; Torquato, S.; Steinhardt, P.J. Complete band gaps in two-dimensional photonic quasicrystals. *Phys. Rev. B* **2009**, *80*, 155112. [CrossRef]
25. Kalugin, P.; Katz, A. Electrons in deterministic quasicrystalline potentials and hidden conserved quantities. *J. Phys. A Math. Theor.* **2014**, *47*, 315206. [CrossRef]
26. Tanese, D.; Gurevich, E.; Baboux, F.; Jacqmin, T.; Lemaître, A.; Galopin, E.; Sagnes, I.; Amo, A.; Bloch, J.; Akkermans, E. Fractal Energy Spectrum of a Polariton Gas in a Fibonacci Quasiperiodic Potential. *Phys. Rev. Lett.* **2014**, *112*, 146404. [CrossRef]
27. Gambaudo, J.M.; Vignolo, P. Brillouin zone labelling for quasicrystals. *New J. Phys.* **2014**, *16*, 043013. [CrossRef]
28. Macé, N.; Jagannathan, A.; Kalugin, P.; Mosseri, R.; Piéchon, F. Critical eigenstates and their properties in one- and two-dimensional quasicrystals. *Phys. Rev. B* **2017**, *96*, 045138. [CrossRef]
29. Macé, N.; Laflorencie, N.; Alet, F. Many-body localization in a quasiperiodic Fibonacci chain. *SciPost Phys.* **2019**, *6*, 050. [CrossRef]
30. Sen, A.; Perelman, C.C. A Hamiltonian model of the Fibonacci quasicrystal using non-local interactions: Simulations and spectral analysis. *Eur. Phys. J. B* **2020**, *93*, 67. [CrossRef]
31. Baggioli, M.; Landry, M. Effective Field Theory for Quasicrystals and Phasons Dynamics. *SciPost Phys.* **2020**, *9*, 062. [CrossRef]
32. Jagannathan, A. The Fibonacci quasicrystal: Case study of hidden dimensions and multifractality. *Rev. Mod. Phys.* **2021**, *93*, 045001. [CrossRef]
33. Satija, I.I.; Naumis, G.G. Chern and Majorana modes of quasiperiodic systems. *Phys. Rev. B* **2013**, *88*, 054204. [CrossRef]
34. Ghadimi, R.; Sugimoto, T.; Tohyama, T. Majorana Zero-Energy Mode and Fractal Structure in Fibonacci–Kitaev Chain. *Phys. Soc. Jpn.* **2017**, *86*, 114707. [CrossRef]
35. Varjas, D.; Lau, A.; Pöyhönen, K.; Akhmerov, A.R.; Pikulin, D.I.; Fulga, I.C. Topological Phases without Crystalline Counterparts. *Phys. Rev. Lett.* **2019**, *123*, 196401. [CrossRef]
36. Cao, Y.; Zhang, Y.; Liu, Y.B.; Liu, C.C.; Chen, W.Q.; Yang, F. Kohn-Luttinger Mechanism Driven Exotic Topological Superconductivity on the Penrose Lattice. *Phys. Rev. Lett.* **2020**, *125*, 017002. [CrossRef]
37. Duncan, C.W.; Manna, S.; Nielsen, A.E.B. Topological models in rotationally symmetric quasicrystals. *Phys. Rev. B* **2020**, *101*, 115413. [CrossRef]
38. Liu, T.; Cheng, S.; Guo, H.; Xianlong, G. Fate of Majorana zero modes, exact location of critical states, and unconventional real-complex transition in non-Hermitian quasiperiodic lattices. *Phys. Rev. B* **2021**, *103*, 104203. [CrossRef]
39. Hua, C.B.; Liu, Z.R.; Peng, T.; Chen, R.; Xu, D.H.; Zhou, B. Disorder-induced chiral and helical Majorana edge modes in a two-dimensional Ammann–Beenker quasicrystal. *Phys. Rev. B* **2021**, *104*, 155304. [CrossRef]
40. Fraxanet, J.; Bhattacharya, U.; Grass, T.; Rakshit, D.; Lewenstein, M.; Dauphin, A. Topological properties of the longrange Kitaev chain with Aubry-Andre-Harper modulation. *Phys. Rev. Res.* **2021**, *3*, 013148. [CrossRef]

41. Rosa, M.I.N.; Ruzzene, M.; Prodan, E. Topological gaps by twisting. *Commun. Phys.* **2021**, *4*, 130. [CrossRef]
42. Sarangi, S.; Nielsen, A.E.B. Effect of coordination on topological phases on self-similar structures. *Phys. Rev. B* **2021**, *104*, 045147. [CrossRef]
43. Fan, J.; Huang, H. Topological states in quasicrystals. *Front. Phys.* **2022**, *17*, 13203. [CrossRef]
44. Zhang, Y.; Liu, X.; Belić, M.R.; Zhong, W.; Zhang, Y.; Xiao, M. Propagation Dynamics of a Light Beam in a Fractional Schrödinger Equation. *Phys. Rev. Lett.* **2015**, *115*, 180403. [CrossRef]
45. Elitzur, S.; Moore, G.W.; Schwimmer, A.; Seiberg, N. Remarks on the Canonical Quantization of the Chern–Simons-Witten Theory. *Nucl. Phys. B* **1989**, *326*, 108–134. [CrossRef]
46. Trebst, S.; Troyer, M.; Wang, Z.; Ludwig, A.W.W. A Short Introduction to Fibonacci Anyon Models. *Prog. Theor. Phys. Suppl.* **2008**, *176*, 384–407. [CrossRef]
47. Bratteli, O. Inductive limits of finite-dimensional C^*-algebras. *Trans. Am. Math. Soc.* **1972**, *171*, 195–234. [CrossRef]
48. Davidson, K.R. *C*-Algebras by Example*; Fields Institute Monographs; Fields Institute for Research in Mathematical Sciences: Toronto, ON, Canada, 1996; ISSN 1069-5273.
49. Hannaford, P.; Sacha, K. Condensed matter physics in big discrete time crystals. *AAPPS Bull.* **2022**, *32*, 12. [CrossRef]
50. Connes, A. *Non-Commutative Geometry*; Academic Press: Boston, MA, USA, 1994.
51. Sadun, L. Tilings, tiling spaces and topology. *Philos. Mag.* **2006**, *86*, 875–881. [CrossRef]
52. Tasnadi, T. Penrose Tilings, Chaotic Dynamical Systems and Algebraic K-Theory. *arXiv* **2002**, arXiv:math-ph/0204022.
53. Jones, V.F.R. Index for Subfactors. *Invent. Math.* **1983**, *72*, 1–26. Available online: http://eudml.org/doc/143011 (accessed on 1 January 2022). [CrossRef]
54. Kauffman, L.H.; Lomonaco, S.J. Braiding, Majorana fermions, Fibonacci particles and topological quantum computing. *Quantum Inf. Process.* **2018**, *17*, 201. [CrossRef]
55. Goodman, F.M.; Wenzl, H. The Temperley-Lieb algebra at roots of unity. *Pac. J. Math.* **1993**, *161*, 307–334. [CrossRef]
56. Feiguin, A.; Trebst, S.; Ludwig, A.W.W.; Troyer, M.; Kitaev, A.; Wang, A.; Freedman, M.H. Interacting Anyons in Topological Quantum Liquids: The Golden Chain. *Phys. Rev. Lett.* **2007**, *98*, 160409. [CrossRef]
57. Zhang, H.; Liu, C.X.; Gazibegovic, S.; Xu, D.; Logan, J.A.; Wang, G.; van Loo, N.; Bommer, J.D.; de Moor, M.W.; Car, D.; et al. Retraction Note: Quantized Majorana conductance. *Nature* **2021**, *591*, E30. [CrossRef]
58. Gazibegovic, S.; Car, D.; Zhang, H.; Balk, S.C.; Logan, J.A.; De Moor, M.W.; Cassidy, M.C.; Schmits, R.; Xu, D.; Wang, G.; et al. RETRACTED ARTICLE: Epitaxy of advanced nanowire quantum devices. *Nature* **2017**, *548*, 434–438. [CrossRef]
59. Zhang, Y.; Wu, Z.; Belić, M.R.; Zheng, H.; Wang, Z.; Xiao, M.; Zhang, Y. Photonic Floquet topological insulators in atomic ensembles. *Laser Photonics Rev.* **2015**, *9*, 331–338. [CrossRef]
60. Flouris, K.; Jimenez, M.M.; Debus, J.D.; Herrmann, H.J. Confining massless Dirac particles in two-dimensional curved space. *Phys. Rev. B* **2018**, *98*, 155419. [CrossRef]
61. Zhang, Z.; Wang, R.; Zhang, Y.; Kartashov, Y.V.; Li, F.; Zhong, H.; Guan, H.; Gao, K.; Li, F.; Zhang, Y.; et al. Observation of edge solitons in photonic graphene. *Nat. Commun.* **2020**, *11*, 1902. [CrossRef] [PubMed]
62. Saraswat, V.; Jacobberger, R.M.; Arnold, M.S. Materials Science Challenges to Graphene Nanoribbon Electronics. *ACS Nano* **2021**, *15*, 3674–3708. [CrossRef] [PubMed]